RSC Advances

PAPER

View Article Online
View Journal | View Issue

Cite this: *RSC Adv.*, 2018, **8**, 6752

Novel N-doped ZrO_2 with enhanced visible-light photocatalytic activity for hydrogen production and degradation of organic dyes

Yuanyang Wang,[a] Yinghua Zhang,[a] Haiqiang Lu,*[a] Yanxin Chen,[a] Zhenmin Liu,[a] Shen Su,[a] Yongbing Xue,[a] Jianfeng Yao *[b] and Hongbo Zeng *[ac]

Two new types of N-doped ZrO_2 photocatalysts ZON and AZON have been synthesized using ethylenediamine as the nitrogen source by a facile and low-cost sol–gel method. The N-doped ZrO_2 samples have been characterized using various techniques including X-ray diffraction (XRD), UV-Vis spectroscopy, Fourier transform infrared spectroscopy (FTIR), X-ray photoelectron spectroscopy (XPS), photoluminescence spectroscopy (PL) and N_2 adsorption–desorption tests. The XRD analysis shows that the crystallinity of ZON samples calcined at 400–600 °C can be indexed to monoclinic ZrO_2; while the AZON samples calcined at 400–550 °C only show amorphous diffraction patterns. The UV-Vis response of both N-doped ZrO_2 samples can be extended to the visible light regime. The high resolution XPS spectra indicate that N element has been doped in the lattice of ZrO_2. Visible-light photocatalytic reactions using the N-doped ZrO_2 photocatalysts (*i.e.* ZON, AZON) calcined at 450 °C show the highest hydrogen production rate (2.12 mmol g^{-1} h^{-1}) and best methylene orange degradation performance due to substitutional N-doping of the ZrO_2. The novel N-doped ZrO_2 materials are demonstrated to be very promising photocatalysts with enhanced visible-light photocatalytic activity. Our results provide useful insights into the development of novel photocatalytic materials for hydrogen production and degradation of organic wastes by narrowing the wide bandgap of semiconductors with high photocatalytic activity under UV-Vis light.

Received 13th December 2017
Accepted 5th February 2018

DOI: 10.1039/c7ra12938f

rsc.li/rsc-advances

1. Introduction

Developing and using renewable energy sources, instead of fossil fuel, has received much research attention over the past two decades, and is believed to be an effective approach to address the environmental and energy challenges facing the world in the 21st century. Hydrogen is a clean and no carbon energy source with great potential for solving the environmental crisis and energy shortage issues.[1–6] Heterogeneous photocatalysis for water splitting into H_2 using semiconducting catalysts has received considerable attention due to its significant economic and environmental benefits in producing clean H_2 from water *via* solar energy.[7] In general, semiconductors possessing electronic structure characterized by a filled valence band (VB) and an empty conduction band (CB) can act as photocatalysts for light-induced photochemical reactions. The prerequisite for an efficient semiconductor photocatalyst is that the redox potential for the evolution of hydrogen and oxygen from water and for the formation of reactive oxygenated species (hydrogen peroxide, hydroxyl, and superoxide radicals) should lie within the band gap of the semiconductor.[8]

During the past 40 years, various semiconductor photocatalytic materials have been developed to split water into H_2 and O_2 under UV and visible light illumination. Splitting water into H_2 and O_2 under sunlight allows the production of clean and renewable H_2 on a large scale. TiO_2 is an n-type semiconductor with bandgap energy of 3.0–3.2 eV, and it is widely used as a heterogeneous photocatalyst for solar applications including production of H_2 from water.[9–17] Zirconia (ZrO_2) is a very important material in petroleum industry for the deformation, dehydrogenation and isomerization of organic compounds,[18] and it has outstanding properties such as high dielectric constant, wide optical band gap, high chemical and thermal stabilities, low optical loss and high transparency in visible and near-infrared regimes.[19] However, zirconia with bandgap energy of 5.0 eV is less used in photocatalysis, especially for applications under sunlight. Several studies reported that incorporation of some transition metal ions could effectively enhance the efficiency of ZrO_2 based catalytic systems.[18,20–24] Nitrogen doping of oxide semiconductors by bandgap modulation of photocatalysts, such as TiO_2 (3.0–

[a]School of Chemical and Biological Engineering, Taiyuan University of Science and Technology, Taiyuan 030024, China. E-mail: luhaiqiang-1900@163.com
[b]College of Chemical Engineering, Nanjing Forestry University, Nanjing 210037, China. E-mail: jfyao@njfu.edu.cn
[c]Department of Chemical and Materials Engineering, University of Alberta, Edmonton, Alberta, T6G 1H9, Canada. E-mail: hongbo.zeng@ualberta.ca

3.2 eV)[25] and Ta_2O_5 (4.0 eV),[26,27] has been proved in our previous studies to effectively enhance visible-light absorption. In this work, N-doped ZrO_2 was prepared using ethylenediamine as the nitrogen source by a facile sol–gel method and heat treatment. The heat treatment at a selected temperature could remove the organic residues and keep the N-dopant. The resulting N-doped ZrO_2 was found to significantly enhance H_2 production rate and methyl organic degradation.

2. Experimental methods

2.1. Preparation of N-doped ZrO_xN_y

Two types of N-doped zirconium oxynitride (ZrO_xN_y) were prepared by a sol–gel method. The first type of N-doped ZrO_xN_y was synthesized using an alcoholysis-based sol–gel method similar to that in our previous work.[25,26] In a typical sol–gel synthesis process, 10 g of $ZrO(NO_3)_2$ was dissolved in 60 mL of anhydrous ethanol, followed by the addition of 5 mL of acetylacetone as a stabilizer under continuous stirring for 4 h. 60 mL of ethylenediamine was added into the sol solution and stirred till they gelled. After the gel being aged for 6 d, the yellowish sol was dried at 60 °C for 5 d. The dry gel was then ground and calcined at 350–600 °C for 1 h. The final products were named ZON-350, ZON-400, ZON-450, ZON-500, ZON-550 and ZON-600, respectively, based on the calcination temperature.

The second type of N-doped (aerogel) zirconium oxynitride was prepared using a similar synthesis method as above except the addition of 5 mL of tetraethyl orthosilicate in the solution of $ZrO(NO_3)_2$, ethanol and acetylacetone. The final dry gel was ground and calcined at 400–550 °C for 1 h. The resulting products were named AZON-400, AZON-450, AZON-500, AZON-550, respectively, based on the calcination temperature.

2.2. Characterization of photocatalysts

The phase structure of N-doped zirconium oxynitride was characterized by X-ray diffraction (XRD) using Rigaku MiniFlex II with Cu Kα radiation ($\lambda = 0.1542$ nm) at 40 kV. The UV-Vis absorption spectra were recorded on a Perkin-Elmer Lambda 750 UV/Vis/NIR Spectrometer. X-ray photoelectron spectroscopy (XPS, Thermo ESCALAB 250) was used to examine the surface chemistry of the N-doped ZrO_xN_y samples, coupled with a spherical capacitor analyser and Al Kα ($h\nu = 1486.6$ eV) as the radiation source. Binding energies were calibrated by the C 1s peak at 284.8 eV. The specific surface areas of the N-doped zirconium oxynitride samples were measured by the Brunauer–Emmett–Teller (BET) method employing nitrogen adsorption at 77 K after treating the samples at 100 °C and $\sim 10^{-4}$ Pa for 2 h using a Tristar-3000 apparatus. Scanning electron microscope and energy dispersive X-ray spectroscopy (SEM-EDS) were observed by the Hitachi S-4800 field emission SEM (operated at 15 kV). Room temperature photoluminescence (PL) spectra were recorded on a spectrofluorometer (FluoroMax-4, HORIBA Jobin Yvon) using a Xe lamp as the excitation source.

2.3. Photocatalytic degradation of methyl orange and photocatalysis tests for H_2 generation

Photocatalytic experiments were performed by following a method reported previously.[25,26] The photocatalytic activity was evaluated by the degradation of methyl orange under visible light irradiation (>400 nm) with a 300 W high-pressure xenon arc lamp. In each test, the photocatalyst from photocatalytic water-splitting (0.5 g) was added into 500 mL of 20 mg L^{-1} methyl orange aqueous solution (pH = 5). Oxygen was bubbled into the suspension, and the photocatalytic degradation efficiency and residue of methyl orange was determined by a UV-Vis spectrometer by monitoring the characteristic absorption peak of methyl orange at 464 nm. And photocatalysis tests for H_2 generation, typically, 0.5 g of photocatalyst, chloroplatinic acid (1% Pt) were added into 500 mL of 20 vol% aqueous methanol solution under a Xe lamp (300 W). The amount of H_2 evolved was determined by using a gas chromatograph (GC).

3. Results and discussion

Fig. 1a and b show the corresponding XRD patterns of the two types of nitrogen-doped zirconium oxynitride products ZON and AZON, respectively, calcined at different temperatures. For ZON-350 (calcined at 350 °C), no obvious characteristic peaks appear on the XRD spectrum (Fig. 1a). For ZON-400, ZON-450, ZON-500, ZON-500 and ZON-600 calcined at 400–600 °C (Fig. 1a), all the XRD characteristic peaks at $2\theta = 24.11°$, 28.10°, 30.00°, 31.37°, 35.19° and 50.21° can be indexed to monoclinic ZrO_2 (JCPDS no. 37–1484). No addition peaks of impurities are observed, indicating that the nitrogen-doped zirconium oxynitride products have a single phase with high purity. The sharp diffraction peaks also indicate high crystallinity of these products. In contrast, Fig. 1b shows that for the AZON samples calcined at 400–550 °C, only amorphous diffraction patterns are detected.

Fig. 2a and b show UV-Vis spectra of the two types of N-doped zirconium oxynitride products ZON and AZON prepared at

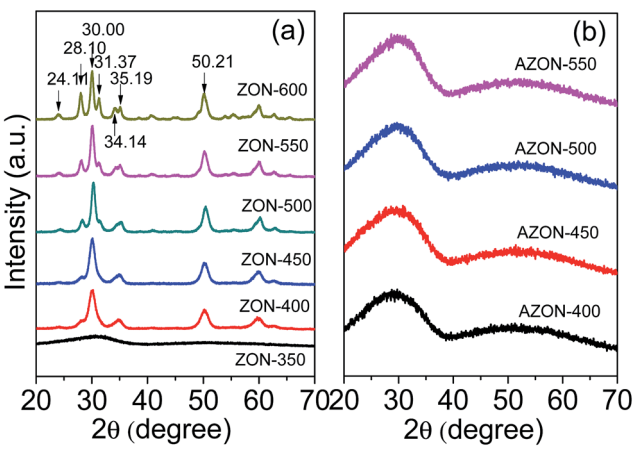

Fig. 1 XRD patterns of different N-doped zirconium oxynitride products: (a) ZON prepared at 350–600 °C, and (b) AZON prepared at 400–550 °C.

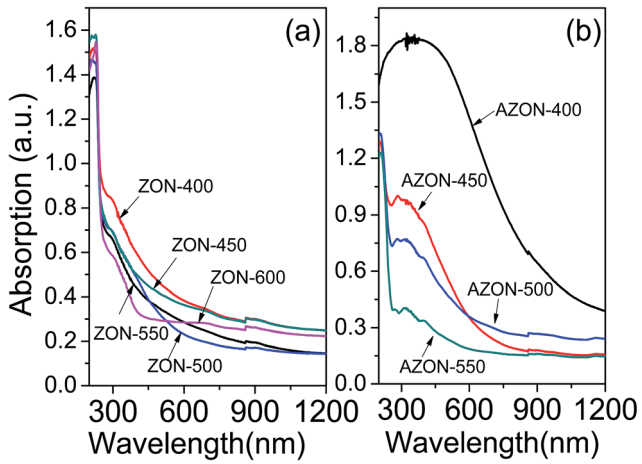

Fig. 2 UV-Visible spectra of (a) ZON and (b) AZON calcined at different temperatures.

different temperatures. Previous study has shown that the band gap of ZrO_2 nanocrystals is about 5.0 eV, and the only UV-Vis response appears at 240 nm. Interestingly, Fig. 2 shows the UV-Vis response of N-doped zirconium oxynitride calcined at 400–600 °C is extended to visible light and near IR regime. As the organic residuals and N-doping element are prone to be oxidized at high temperature, the absorbance threshold in visible light becomes weaker and the absorption edge shifts to shorter wavelength with increasing the calcination temperature for both ZON and AZON materials.

Fig. 3a shows the FTIR spectra of N-doped ZON nanocrystals in the range from 400 to 2500 cm^{-1}. The bands at ~569 and 483 cm^{-1} can be attributed to the Zr–O and Zr–O–Zr vibrations, respectively.[28] The bands at ~1621 cm^{-1} can be ascribed to the O–H vibrations of H_2O absorbed in the N-doped ZON nanocrystals. The bands at ~1341 cm^{-1} can be attributed to the metal and hydroxide bond (Zr–OH).[29] As can be seen, additional peaks are observed after doping with N. The weak peaks at ~742 cm^{-1} are associated with the wagging vibration of N–H bond, while the peaks at 1570 cm^{-1} are associated with their

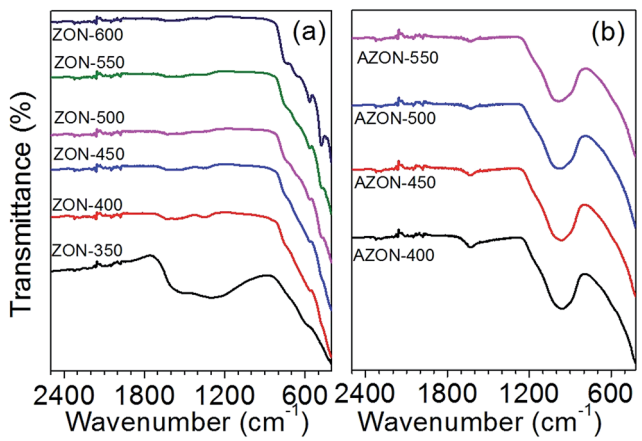

Fig. 3 FTIR spectra of (a) ZON and (b) AZON prepared at different temperatures.

bending mode.[29] The band at 1341 cm^{-1} can be ascribed to the δ_{C-H} of the carboxylate group.[30] The FTIR spectra in Fig. 3a suggest that carbon-related impurities are present in the ZON samples calcined at low temperature (*e.g.* 350 °C), which can be removed at high temperature. However, for AZON samples, the FTIR spectra in Fig. 3b show that only the bands at ~1621 and 985 cm^{-1} can be detected, and other vibrations are too weak to be detected. The band at ~1000 cm^{-1} can be assigned to the Si–O–Zr vibration.[31]

XPS is widely used for the characterization of surface elemental composition and electronic states of photocatalysts. As shown in Fig. 4a, the global XPS survey spectra of ZON and AZON prepared at different temperatures indicate the presence of Zr, O, N and C elements and some peaks of other elements, such as Si, were observed. The C 1s peak is located at 285.4 eV, which is possibly ascribed to the remaining organic precursor of all samples not yet completely removed at temperatures less than 550 °C. Fig. 4a displays the spectra of all samples for Zr consist of Zr 4p, Zr 3d, Zr 3p3, Zr 3p1, Zr 3s at 31.1, 182.5, 331.9, 347.2, 433.3 eV, respectively.[32] Only amorphous diffraction patterns of AZON sample calcined at 450 °C was detected by XRD. However, AZON sample calcined at 450 °C was fitted by a single component (Zr–O) with the binding energy of 182.7 eV for the Zr $3d_{5/2}$ (Fig. 4b). The high resolution XPS spectra of N 1s region of the catalysts are shown in Fig. 4c. There is one main peak centered at 396.8 eV in the XPS spectrum of N–ZrO_2, corresponding to the Zr–N bond. There is also an additional peak at higher (400 eV) binding energy compared to the main peak. This characteristic peak is assigned to the N–O bond for the Zr–O–N state.[29] To fit O 1s spectrum, two components (O–Zr and O–H) were required. Fig. 4d shows that the binding energies for them were 530.4 and 532.2 eV, respectively.[33]

Fig. 5a shows the element components of AZON-450 sample. The EDS patterns of the sample after N doping, it is obviously that the peak of N element appeared by calcined at 450 °C. Fig. 5b shows the SEM image and corresponding elemental mapping and the elements Zr, Si, O, C, N are distributed in the sample. Very importantly, the N signal is observed in the image, which means AZON-450 sample was doped by the nitrogen element. The elemental compositions of ZON (Fig. 5c) and AZON (Fig. 5d) by SEM-EDS were summarized. N-doped ZrO_2 was prepared using ethylenediamine as the nitrogen source by sol–gel method and heat treatment. N doping level in visible light-responsive photocatalysts will affect the visible photocatalytic activity of samples. From the EDS analysis, the ZON-450 AND AZON-450 possessed the highest nitrogen content, which reached 1.24% and 1.15%, respectively.

Fig. 6a and b shows photoluminescence spectra of ZON and AZON samples, respectively, at room temperature. Photoluminescence excitation peaks were selected according to the UV-Vis absorption spectra ($\lambda_{max} = 290$ nm). The emission peaks of all the ZON and AZON samples are centered at 425–475 nm when the sample is excited at 290 nm with clear shift. Fig. 6 shows that the intensity of PL peaks overall increases with increasing the calcination temperature. It is noted that ZON-450 and AZON-450 samples calcined at 450 °C exhibit the lowest photoluminescence signal among all the spectra for ZON and

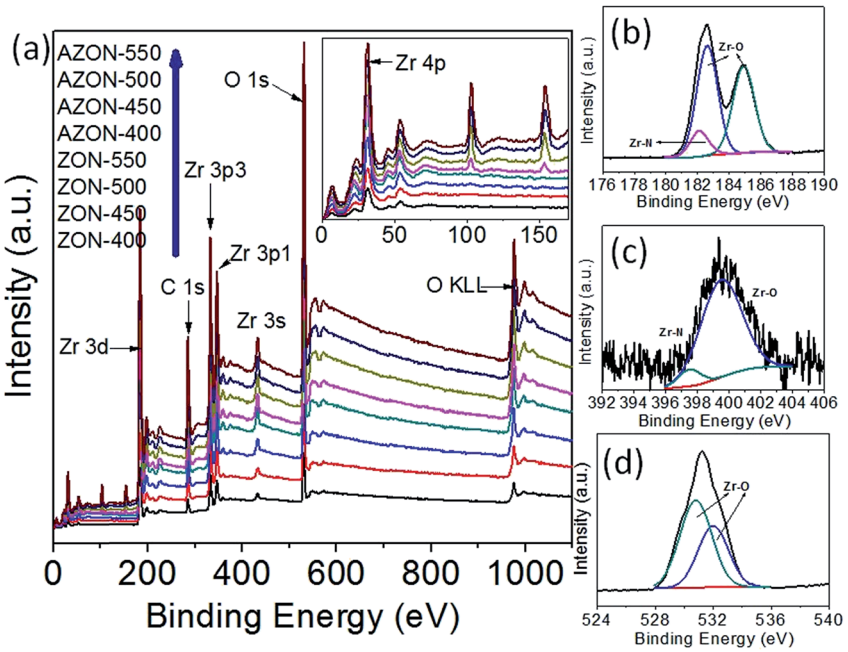

Fig. 4 XPS survey of ZON and AZON prepared at different temperatures (a), high resolution spectrum of AZON sample calcined at 450 °C of Zr 3d (b), N 1s peak around the 396.8 eV regions (c), O 1s (d).

AZON samples, respectively, which indicates the recombination rate of photogenerated charge carriers is the lowest on the surfaces of ZON-450 and AZON-450 samples. The PL results thus confirm that the N-doped zirconium oxynitride sample with a lower PL displays a higher photocatalytic activity.

The surface area and pore size distribution of N-doped zirconium oxynitride samples (ZON and AZON) were characterized by Brunauer–Emmett–Teller (BET) measurements. Fig. 7a shows the nitrogen adsorption–desorption isotherm of ZON samples, indicating the presence of meso- and macroporous structure. The BET surface area of ZON samples decreases from 31 to 16 $m^2 g^{-1}$ as the calcination temperature increases from 400 to 550 °C, which should arise from the high crystallinity of ZON samples calcined at a high temperature, and the peak pore size is centered at around 8.2–20.3 nm (Fig. 7a inset). The nitrogen adsorption–desorption isotherm of AZON samples is a typical type IV curve, indicating the presence of mesoporous structure. The BET surface area of AZON samples decreases from 290 to 217 $m^2 g^{-1}$ as the calcination temperature increases from 400 to 550 °C, and the peak pore size is centered at around 2.4–3.3 nm (Fig. 7b inset). The larger pore size of ZON samples should arise from the intra-crystalline pore, while the relatively smaller pore size of AZON samples should arise from carcase construction.

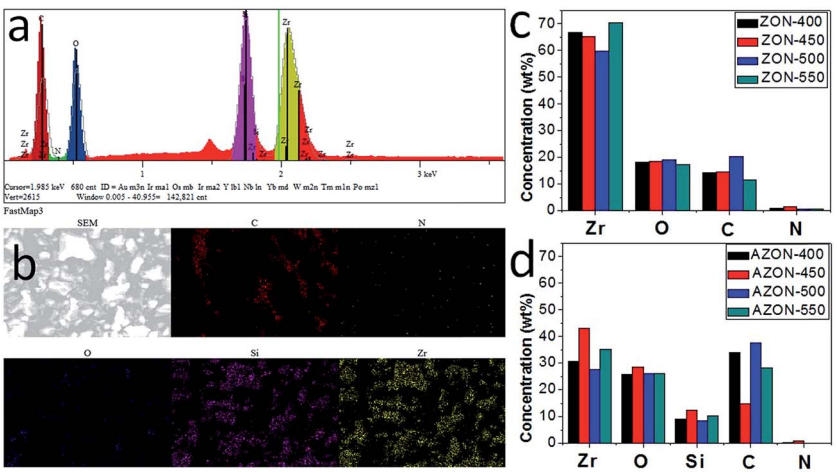

Fig. 5 SEM-EDS spectrum (a) and corresponding elemental mapping (b) of AZON-450 sample, the elemental compositions of ZON samples (c) and AZON samples (d) by SEM-EDS.

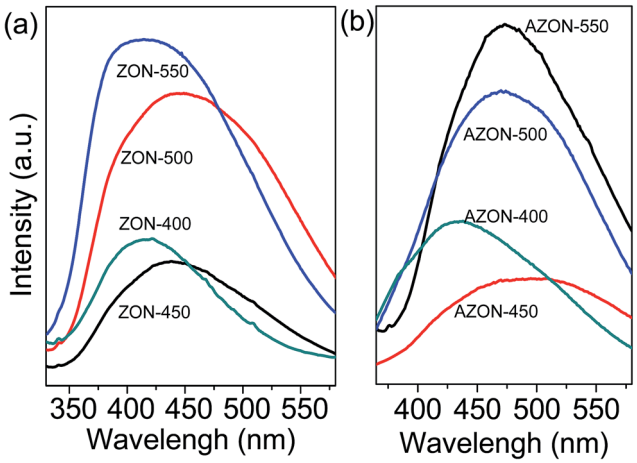

Fig. 6 Photoluminescence spectra of (a) ZON and (b) AZON samples calcined at different temperatures, with excitation wavelength 290 nm.

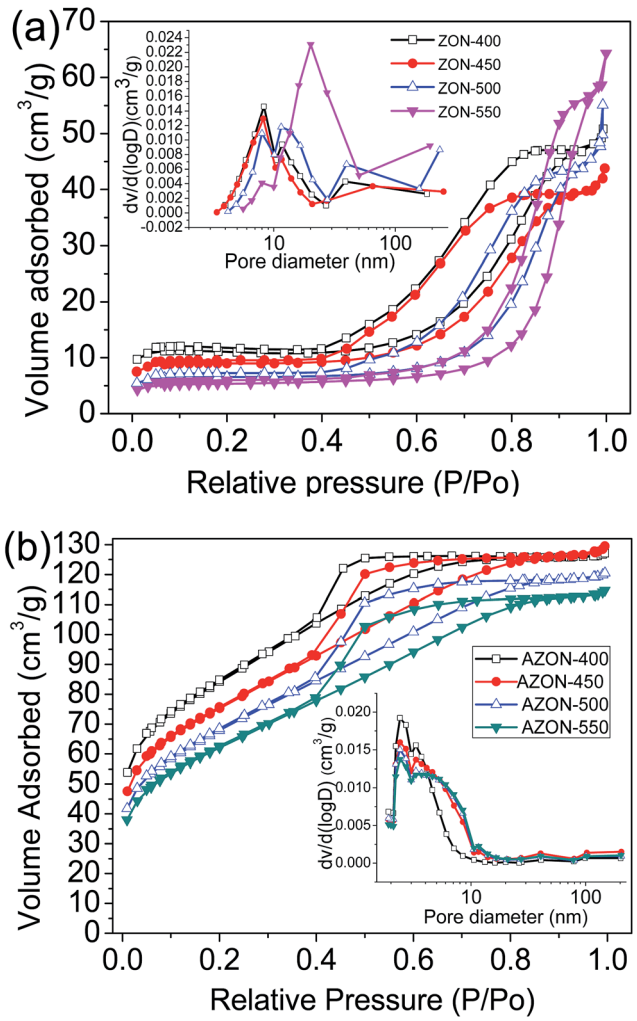

Fig. 7 N_2 adsorption–desorption isotherms and pore size distributions (inset) of (a) ZON and (b) AZON samples calcined at different temperatures.

Methylene orange was used as the model organic pollutant to evaluate the photocatalytic activity of the N-doped ZrO_2 samples. Fig. 8a shows the visible-light induced photocatalytic degradation of methylene orange over different N-doped ZrO_2 photocatalysts. Almost all the N-doped ZrO_2 samples exhibit the visible-light photocatalytic activity, suggesting that the ethylenediamine is an effective N source. ZON and AZON samples calcined at 450 °C show the highest photocatalytic activity in the photocatalytic degradation of methylene orange, which indicates that the sintering temperature also plays an important key role in the photocatalytic activity of N-doped ZrO_2 samples. Fig. 8b shows that ZON-450 has the highest H_2 generation rate as high as 2.12 mmol g^{-1} h^{-1} and AZON-450 has a H_2 generation rate of 1.85 mmol g^{-1} h^{-1}. The photocatalytic H_2 tests further supported the excellent photocatalytic activity of the N-doped ZrO_2 materials, as shown in Fig. 8b. It is noted that although the ZON and AZON samples calcined at 450 °C show slightly lower photocatalytic activity in the H_2 generation tests than the TiON-500 and TaO_xN_y-550 as we reported previously,[25,26] the photocatalytic results for the novel ZrO_2 based photocatalysts (*i.e.* ZON and AZON) with very high bandgap

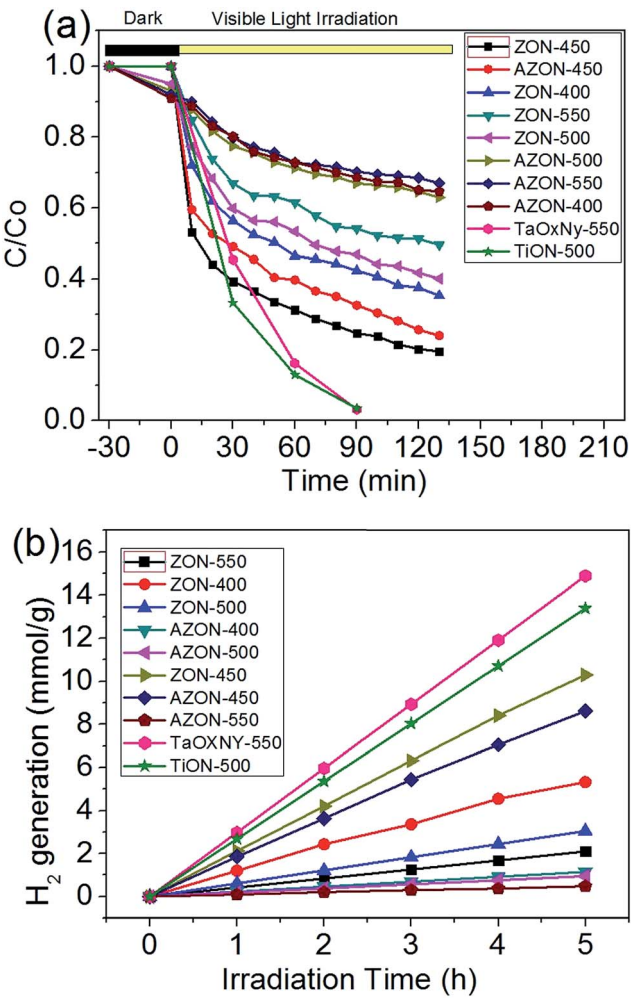

Fig. 8 (a) Photocatalytic degradation of methyl orange and (b) H_2 generation on ZON and AZON samples sintered at 400–550 °C.

(5.0 eV) are of both fundamental and practical importance. Among the various photocatalysts available, the low-cost and facilely synthesized N-doped ZrO_2 materials have high stability against photocorrosion and high negative value of conduction band potential (−1.0 eV) with strong oxidation power, which are more suitable for the degradation of a wide variety of organic pollutants and hydrogen production through solar-driven catalytic process.

4. Conclusions

Two types of N-doped zirconium oxynitride (ZrO_xN_y) have been prepared using ethylenediamine as the N source by a facile sol–gel method, and show enhanced photocatalytic activity for the degradation of methylene orange and hydrogen production under visible light irradiation. The XRD analysis shows that the crystallinity of ZON samples calcined at 400–600 °C can be indexed to monoclinic ZrO_2, and for AZON samples calcined at 400–550 °C, only amorphous diffraction patterns are detected. The UV-Vis response of ZON and AZON samples calcined at 400–600 °C is extended to visible light regime. The high resolution XPS spectra of samples calcined at 450 °C indicate that N element has been doped in the lattice of ZrO_2. An appropriate high temperature (450 °C) heat treatment removes most of the organic residues and keeps the N-dopant, which endows the N-doped zirconium oxynitride photocatalysts the highest hydrogen production rate and methylene orange degradation performance among all the samples calcined under varying temperature. The novel N-doped ZrO_2 materials have been demonstrated to be very promising photocatalysts with enhanced visible-light photocatalytic activity. Our results provide useful insights into the development of novel photocatalytic materials for hydrogen production and degradation of organic wastes by narrowing wide bandgap of semiconductors with high photocatalytic activity under UV-Vis light.

Conflicts of interest

There are no conflicts to declare.

Acknowledgements

This research was financially supported by Basic Condition Platform Construction Program of Shanxi Province (No. 2012091019), Science and Technology Plan of Jincheng City (No. 201501004-18), Key Research Plan of Social Development of Shanxi Province (No. 201603D321017) and Scientific Research Foundation of Taiyuan University of Science and Technology (No. 20112004). J. Y. thanks the financial support from Natural Science Key Project of the Jiangsu Higher Education Institutions (15KJA220001). H. Zeng gratefully acknowledges the support from the Natural Sciences and Engineering Research Council of Canada (NSERC).

References

1 P. Yang, H. Ou, Y. Fang and X. Wang, *Angew. Chem., Int. Ed.*, 2017, **56**, 3992–3996.
2 Y. Wang, Q. Wang, X. Zhan, F. Wang, M. Safdar and J. He, *Nanoscale*, 2013, **5**, 8326–8339.
3 L. K. Putri, W.-J. Ong, W. S. Chang and S.-P. Chai, *Appl. Surf. Sci.*, 2015, **358**, 2–14.
4 X. F. Zhang, Y. Z. Chen, Y. Feng, X. G. Zhang, J. H. Qiu, M. M. Jia and J. F. Yao, *J. Alloys Compd.*, 2017, **705**, 392–398.
5 J. Zhang, Y. Wang, J. Jin, J. Zhang, Z. Lin, F. Huang and J. Yu, *ACS Appl. Mater. Interfaces*, 2013, **5**, 10317–10324.
6 R. S. Sprick, J. X. Jiang, B. Bonillo, S. Ren, T. Ratvijitvech, P. Guiglion, M. A. Zwijnenburg, D. J. Adams and A. I. Cooper, *J. Am. Chem. Soc.*, 2015, **137**, 3265–3270.
7 A. A. Ismail and D. W. Bahnemann, *Sol. Energy Mater. Sol. Cells*, 2014, **128**, 85–101.
8 S. G. Kumar and L. G. Devi, *J. Phys. Chem. A*, 2011, **115**, 13211–13241.
9 Q. Wu, W. Li, D. Wang and S. Liu, *Appl. Surf. Sci.*, 2014, **299**, 35–40.
10 B. Yuan, Y. Wang, H. Bian, T. Shen, Y. Wu and Z. Chen, *Appl. Surf. Sci.*, 2013, **280**, 523–529.
11 W. Q. Li, X. Liu and H. X. Li, *J. Mater. Chem. A*, 2015, **3**, 15214–15224.
12 J. H. Qiu, Y. Feng, X. F. Zhang, X. G. Zhang, M. M. Jia and J. F. Yao, *RSC Adv.*, 2017, **7**, 10668–10674.
13 S. Mansingh, D. Padhi and K. Parida, *Catal. Sci. Technol.*, 2017, **7**, 2772–2781.
14 S. Pany and K. Parida, *ACS Sustainable Chem. Eng.*, 2014, **2**, 1429–1438.
15 G. K. Pradhan, N. Sahu and K. Parida, *RSC Adv.*, 2013, **3**, 7912–7920.
16 G. Mishra, K. Parida and S. Singh, *ACS Sustainable Chem. Eng.*, 2015, **3**, 245–253.
17 B. Naik, K. Parida and C. S. Gopinath, *J. Phys. Chem. C*, 2010, **114**, 19473–19482.
18 L. Renuka, K. S. Anantharaju, S. C. Sharma, H. P. Nagaswarupa, S. C. Prashantha, H. Nagabhushana and Y. S. Vidya, *J. Alloys Compd.*, 2016, **672**, 609–622.
19 Y. Xie, A. N. Zhou, Y. T. Zhang, Y. P. Huo, S. F. Wang and J. M. Zhang, *J. Magn. Magn. Mater.*, 2015, **387**, 58–61.
20 S. Stojadinović, N. Tadić and R. Vasilić, *Mater. Lett.*, 2016, **164**, 329–332.
21 L. X. Lovisa, V. D. Araújo, R. L. Tranquilin, E. Longo, M. S. Li, C. A. Paskocimas, M. R. D. Bomio and F. V. Motta, *J. Alloys Compd.*, 2016, **674**, 245–251.
22 A. O. de Souza, F. F. Ivashita, V. Biondo, A. Paesano and D. H. Mosca, *J. Alloys Compd.*, 2016, **680**, 701–710.
23 I. M. Mohamed, V.-D. Dao, A. S. Yasin, H. M. Mousa, M. A. Yassin, M. Y. Khan, H.-S. Choi and N. A. Barakat, *Mater. Charact.*, 2017, **127**, 357–364.
24 Y. Sun, L. Chen, Y. Bao, G. Wang, Y. Zhang, M. Fu, J. Wu and D. Ye, *Catal. Today*, 2017, DOI: 10.1016/j.cattod.2017.04.017.
25 H. Li, Y. Hao, H. Lu, L. Liang, Y. Wang, J. Qiu, X. Shi, Y. Wang and J. Yao, *Appl. Surf. Sci.*, 2015, **344**, 112–118.
26 Y. Wang, H. Q. Lu, Y. Y. Wang, J. H. Qiu, J. Wen, K. Zhou, L. Chen, G. Song and J. F. Yao, *RSC Adv.*, 2016, **6**, 1860–1864.
27 T. Takata, C. Pan and K. Domen, *ChemElectroChem*, 2016, **3**, 31–37.

28 J. M. E. Matos, F. A. Júnior, L. S. Cavalcante, V. Santos, S. H. Leal, L. S. Júnior, M. R. M. C. Santos and E. Longo, *Mater. Chem. Phys.*, 2009, **117**, 455–459.
29 H. Sudrajat, S. Babel, H. Sakai and S. Takizawa, *J. Environ. Manage.*, 2016, **165**, 224–234.
30 H. Zheng, K. Y. Liu, H. Q. Cao and X. R. Zhang, *J. Phys. Chem. C*, 2009, **113**, 18259–18263.
31 Q. Wang, X. Li, W. Fen, H. Ji, X. Sun and R. Xiong, *J. Porous Mater.*, 2014, **21**, 127–130.
32 Y. C. Xin, C. L. Liu, K. F. Huo, G. Y. Tang, X. B. Tian and P. K. Chu, *Surf. Coat. Technol.*, 2009, **203**, 2554–2557.
33 J. W. Liu, M. Y. Liao, M. Imura, A. Tanaka, H. Iwai and Y. Koide, *Sci. Rep.*, 2014, **4**, 6395.